First-principles molecular dynamics study of glassy GeS2: Atomic structure and bonding properties

M. Celino, S. Le Roux, Guido Ori, Benoit Coasne, A. Bouzid, M. Boero, C. Massobrio

First-principles molecular dynamics study of glassy GeS_2: Atomic structure and bonding properties

M. Celino,[1] S. Le Roux,[2] G. Ori,[3,4] B. Coasne,[3,4] A. Bouzid,[2] M. Boero,[2] and C. Massobrio[2]

[1]*ENEA, C. R. Casaccia, Via Anguillarese 301, I-00123 Rome, Italy*

[2]*Institut de Physique et de Chimie des Matériaux de Strasbourg, 23 Rue du Loess, Boîte Postale 43, F-67034 Strasbourg Cedex 2, France*

[3]*Institut Charles Gerhard Montpellier, ENSCM, Université Montpellier 2, 8 Rue de l'Ecole Normale, F-34296 Montpellier Cedex 5, France*

[4]*Multiscale Material Science for Energy and Environment, UMI 3466 CNRS-MIT, 77 Massachusetts Avenue, Cambridge Massachusetts, USA*

(Received 23 May 2013; revised manuscript received 15 October 2013; published 4 November 2013)

The structure of glassy GeS_2 is studied in the framework of density functional theory, by using a fully self-consistent first-principles molecular dynamics (FPMD) scheme. A comparative analysis is performed with previous molecular dynamics data obtained within the Harris functional (HFMD) total energy approach. The calculated total neutron structure factor exhibits an unprecedented agreement with the experimental counterpart. In particular, the height of the first sharp diffraction peak (FSDP) improves considerably upon the HFMD results. Both the Ge and the S subnetworks are affected by a consistent number of miscoordinations, coexisting with the main tetrahedral structural motif. Glassy GeS_2 features a short-range order quite similar to the one found in glassy $GeSe_2$, a notable exception being the larger number of edge-sharing connections. An electronic structure localization analysis, based on the Wannier functions formalism, provides evidence of a more enhanced ionic character in glassy GeS_2 when compared to glassy $GeSe_2$.

DOI: 10.1103/PhysRevB.88.174201 PACS number(s): 61.43.Fs, 61.25.Em, 61.20.Ja, 71.15.Pd

I. INTRODUCTION

Amorphous germanium disulfide (a-GeS_2) belongs to the class of AX_2 (A = Ge, Si; X = O, Se, S) disordered materials largely employed on the technological side since very much prone to a widespread range of applications.[1] Over the years, chalcogenide glasses have been incorporated into several devices such as optical materials (lasers, fiber optics, and optical lenses for infrared transmission), sensitive media for optical recording, re-writable discs, and nonvolatile memory devices.[2–4] Some germanium-based chalcogenide systems, including sulfide ones, are known to exhibit excellent Li^+, Ag^+, and Cu^{2+} conductivity while simultaneously maintaining relatively good thermal stability.[5,6] The high ionic conductibility of silver doped germanium sulfide materials is used in conductive bridging random access memory (CBRAM), expected to greatly improve the performance of memory devices, at lower costs and energy consumption.[7]

In view of the potential application of these glasses, compelling need for a thorough structural characterization is a priority for both the experimental and the atomic scale modeling approaches. Focusing on glassy $GeSe_2$ (g-$GeSe_2$, g standing hereafter for glass) and g-GeS_2, it appears that the former has received much more attention than the latter, despite the fact that both are prototypical models of tetrahedral networks featuring intermediate range order (IRO), involving scales well beyond nearest neighbor distances.[8–13] For these network topologies, IRO manifests itself through the appearance of the first sharp diffraction peak (FSDP) at low wave vectors in the total neutron structure factor.[14]

A first issue to be addressed to unravel the kind of atomic-scale connectivity is the extent of chemical order. That amounts to assessing quantitatively the proportion of homopolar bonds and/or miscoordinations. We recall that at the GeS_2 stoichiometry perfect chemical order corresponds to the absence of any Ge (Se,S) atoms not fourfold (twofold) coordinated. While the presence of homopolar bonds in g-$GeSe_2$ has long been established,[15] some controversy appeared on the existence of these defects in the case of g-GeS_2.[16,17] Indeed, early neutron diffraction data[16] seem to exclude any significant departure from chemical order, predicted by a set of Raman and calorimetry data.[17] More recently, a set of x-ray and neutron diffraction measurements provided new evidence for the absence of homopolar bonds, thereby pointing out a structural difference between g-$GeSe_2$ and g-GeS_2.[18]

On the atomic-scale modeling side, a detailed study of g-GeS_2 has been produced by Jund and coworkers. By relying on a non-self-consistent density functional theory approach [Harris functional implemented within the local density approximation (LDA)] and using molecular dynamics, these authors have elucidated structural, vibrational, and electronic properties on periodic models of 96 and 258 atoms.[8,9,19] This approach will be termed HFMD hereafter. Evidence was provided for the existence of small amounts of homopolar bonds (at least in the $N = 258$ sample) and threefold coordinated sulfur atoms.[8,9]

The question arises on how the performances of the HFMD approach compare with those of the fully self-consistent density functional-based first-principles molecular dynamics (FPMD). Within this latter scheme, it has been shown that disordered chalcogenide models are very sensitive to the details of the electronic structure framework, due to delicate interplay between the ionic and the covalent characters.[12] In particular, a firm assessment has been reached in the case of Ge_xSe_{1-x} systems, for which structural and electronic properties were found to be better described by exchange-correlation recipes enhancing the electron localization properties.[12] To date, no FPMD results are available for g-GeS_2. This paper is intended to fill this gap through the use of the same theoretical ingredients (first-principles molecular dynamics based on fully self-consistent density functional theory) exploited in the past for the $GeSe_2$ and other Ge_xSe_{1-x} disordered networks.[12,13,20–24] We are interested in elucidating the structural properties through an analysis in real and reciprocal space of the appropriate quantities (in particular pair

correlation functions and partial/total structure factors). The careful comparison carried out with the previous HFMD study provides a view on the performances of the FPMD and HFMD approaches, thereby allowing one to extract information on the analogies and differences encountered in the description of bonding.

This paper is organized as follows. In Sec. II, we describe how we generated our model structures of a-GeS_2. Our results are collected in three sections, which are devoted to real space properties (Sec. III), reciprocal space properties (Sec. IV), and electronic properties (Sec. V). Conclusive remarks can be found in Sec. VI.

II. THEORETICAL MODEL

We adopted the method by Car and Parrinello to ensure a self-consistent evolution of the electronic structure during the molecular dynamics motion.[25] The CPMD code was employed for this purpose.[26] Our simulations were performed on a system containing $N = 480$ (160 Ge and 320 S) atoms in a periodically repeated cubic cell of size 23.58 Å, corresponding to the experimental density of g-GeS_2 (2.75 g/cm^3) at room temperature.[27] This size ensures a safe compromise between the proper account of intermediate range order distances and an affordable computational cost. It is worth mentioning the fact that for the prototypical case of liquid $GeSe_2$, the increase of the system size from $N = 120$ to $N = 480$ does not alter significantly the structural information obtained for the smaller system.[23]

The electronic structure was described in the framework of density functional theory (DFT) with the generalized gradient approximation (GGA) due to Becke (B) for the exchange energy and Lee, Yang, and Parr (LYP) for the correlation energy.[28,29] For the case of chalcogenides, we refer to Ref. 12 for a detailed account of the reasons underlying the better performances of the BLYP approach when compared to the Perdew and Wang scheme.[30] In short, we recall that the BLYP approach was found to improve upon the PW one in the case of short-range properties of Ge-Se networks where the tetrahedral coordination is predominant. It turns out that Ge−Ge interaction is better reproduced due to a better account of electronic localization effects.[12]

In our work, the valence electrons were treated explicitly, in conjunction with norm conserving pseudopotentials of the Trouiller-Martins type to account for core-valence interactions.[31] The wave functions were expanded at the Γ point of the supercell on a plane-wave basis set with an energy cutoff $E_c = 20$ Ry. A fictitious electron mass of 2000 a.u. (i.e., in units of $m_e a_0^2$ where m_e is the electron mass and a_0 is the Bohr radius) and a time step of $\Delta t = 0.24$ fs are adopted to integrate the equations of motion. Temperature control was implemented for both the ionic and electronic degrees of freedom by using Nosé-Hoover thermostats.[32–34]

Four different equilibrium trajectories were generated to obtain the targeted structural properties. In the first three cases, the starting configurations were created by positioning the atoms randomly. To this purpose, the positions responsible for interatomic distances much shorter than the values of the Ge-Ge, S-S, and Ge-S dimers were modified "*ad hoc*." A lower bound of 1.7 Å has been selected for this purpose. We introduced further disorder through annealing at $T = 2000$ K for 10 ps thereby allowing for significant diffusion of both species ($D_\alpha > 10^{-5}$ cm^2/s) and subsequent loss of memory of the initial configuration. The system is gradually quenched at $T = 1200$ K during 9 ps by decreasing the temperature in a stepwise manner with intervals of 100 K. A final quench is performed by setting the temperature to $T = 300$ K for a period of 8 ps, with physical quantities averaged on a trajectory lasting about 6 ps. Overall, the quench rate for the cooling in between T = 2000 K and T = 300 K turns out to be very high, i.e., $q(1)_r^{FPMD} = 5 \times 10^{14}$ K/s. A slower quench rate, $q(2)_r^{FPMD} = 3 \times 10^{13}$ K/s was adopted to generate the fourth trajectory, for which one equilibrated configuration at T = 300 K was taken as starting point. This time, the thermal cycle encompassed 10 ps at T = 300 K, 10 ps at T = 700 K, and 11 ps again at T = 300 K for the production of the averages.

A previous HFMD study on the influence of the quench rate on the properties of this same glass indicates that the salient structural features (as the presence of homopolar bonds) are not dependent on the extent of the quench rate over a large range.[9] In what follows, this same study will be employed to establish a comparison with the present calculations. For sake of consistency, among the HFMD results of Ref. 9, we have selected those obtained for the quench rate closer to $q(1)_r^{FPMD}$. In this paper, reported mean values relative to the first three trajectories will be labeled as FPMD(1). Averages taken over the fourth trajectory will be referred to as FPMD(2). We anticipate that only small differences (a few percent at most) are found among the two sets of results FPMD(1) and FPMD(2), demonstrating that structural properties are not sensitive to changes in the quench rates, at least for the range of values employed.

Analysis of the detailed electronic structure is given in term of the maximally localized Wannier functions.[35,36] Following the standard procedure, the Wannier functions and the corresponding centers are obtained as unitary transformation *on the fly* of the Kohn-Sham orbitals. Specifically, among all the possible unitary transformations, we select the one that minimized the spread,

$$\Omega = \sum_i (\langle i|\mathbf{r}^2|i\rangle - \langle i|\mathbf{r}|i\rangle^2). \tag{1}$$

This leads to an iterative scheme for computing the orbital transformation:

$$w_n(\mathbf{r}) = \sum_i \left[\prod_p \exp\left(-A_{i,n}^p\right) \cdot \psi_i(\mathbf{r}) \right], \tag{2}$$

where p is the order of the iteration as specified in Ref. 35. The Wannier states provide in this way an unbiased method for partitioning the charge density and the electronic information becomes then contracted into four numbers; the center of the orbitalon x is then defined by

$$x_n = -\frac{L}{2\pi} \mathrm{Im} m \log\langle w_n|\exp(-i2\pi \cdot x/L)|w_n\rangle, \tag{3}$$

with similar expressions along the other two Cartesian directions, and its related spread. Here L is the length of the simulation cell along the x direction.

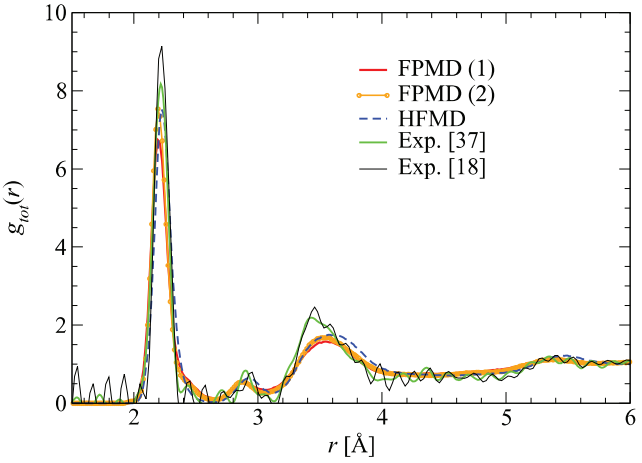

FIG. 1. (Color online) Total pair correlation function of amorphous GeS_2. Comparison among the results from Ref. 9 obtained with the Harris functional (dashed blue line), the present FPMD calculation [thick red line, FPMD(1) and yellow line FPMD(2)], and the experimental measurements from Ref. 37 (green symbols) and Ref. 18 (straight black line).

III. REAL SPACE PROPERTIES

A. Pair correlation functions

In Fig. 1 our total pair correlation functions $g_{\rm tot}^{\rm FPMD}(r)$ [FPMD(1) and FPMD(2)] are compared with the HFMD results of Ref. 9 [$g_{\rm tot}^{\rm HFMD}(r)$] and two experimental data sets [$g_{\rm exp}^{B}(r)$, $g_{\rm exp}^{S}(r)$] due to the teams of Bychkov (Ref. 37) and Salmon (Ref. 18), respectively.

In Table I the first three peaks and minima positions of our total PCF are reported and compared with the two sets of experimental results[37] and HFMD calculations.[9]

Both FPMD results are able to reproduce all the experimental features, such as the number of relevant peaks and their positions. Concerning the intensity, a clear-cut assessment is hampered by the differences between $g_{\rm exp}^{B}(r)$ and $g_{\rm exp}^{S}(r)$, the intensity of the FPMD first peak lying midway between the two experimental data. At this level of comparison, the HFMD and FPMD approaches do not differ significantly, even though the first peak of $g_{\rm tot}^{\rm HFMD}(r)$ is sharper, as a first signature of a stronger tetrahedral network.

In Fig. 2 we show the pair correlation functions $g_{\rm GeGe}^{\rm FPMD}(r)$ [FPMD(1) and FPMD(2)], $g_{\rm GeGe}^{\rm HFMD}(r)$, $g_{\rm GeS}^{\rm FPMD}(r)$ [FPMD(1) and

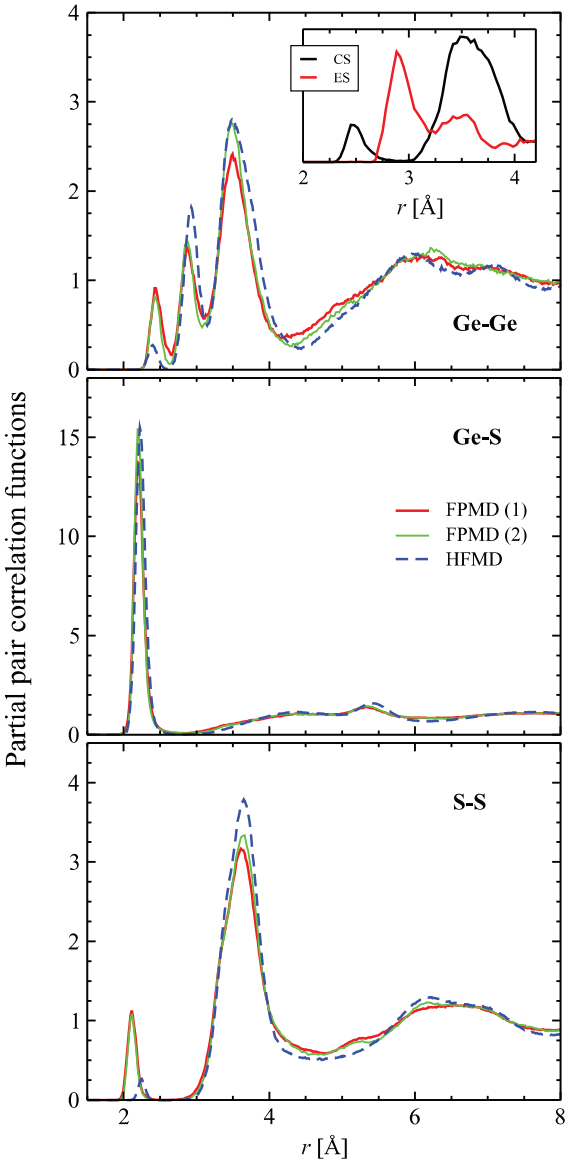

FIG. 2. (Color online) Partial pair correlation functions of amorphous GeS_2. Comparison between the results from Ref. 9 obtained with the Harris functional (dashed blue line), and the present FPMD calculations (thick red line and green line). In the inset the FPMD(1) Ge−Ge correlation is decomposed in the contributions due to edge-sharing and corner-sharing tetrahedra.

TABLE I. First (FP), second (SP), and third (TP) peak positions and first (FM), second (SM), and third (TM) minima positions of total, $g_T(r)$, and partial pair correlation functions $g_{\rm GeGe}(r)$, $g_{\rm GeS}(r)$, and $g_{\rm SS}(r)$. Results for the present works are compared to HFMD[9] and experimental[18,37] counterparts.

Position	$g_{\rm tot}(r)$					$g_{\rm GeGe}(r)$			$g_{\rm GeS}(r)$			$g_{\rm SS}(r)$		
(Å)	FPMD(1)	FPMD(2)	HFMD	Ref. 18	Ref. 37	FPMD(1)	FPMD(2)	HFMD	FPMD(1)	FPMD(2)	HFMD	FPMD(1)	FPMD(2)	HFMD
FP	2.19	2.19	2.22	2.21	2.24	2.44	2.43	2.39	2.19	2.19	2.22	2.11	2.11	2.25
FM	2.67	2.67	2.61	2.59	2.65	2.66	2.63	2.57	2.81	2.89	2.80	2.58	2.58	2.60
SP	2.86	3.06	2.90	2.92	2.94	2.86	2.87	2.93	4.38	–	4.36	3.61	3.66	3.65
SM	2.87	3.05	3.13	3.06	3.14	3.10	3.08	3.15	4.84	4.95	4.97	4.77	4.66	4.67
TP	3.54	3.54	3.56	3.45	3.45	3.50	3.48	3.49	5.34	5.34	5.44	–	–	–
TM	4.15	4.43	4.15	4.00	4.05	4.15	4.31	4.43	6.23	6.45	6.19	–	–	–

FPMD(2)], $g_{GeS}^{HFMD}(r)$, $g_{SS}^{FPMD}(r)$ [FPMD(1) and FPMD(2)], and $g_{SS}^{HFMD}(r)$. Also, in Table I, the main peak maxima and minima of these same pair correlation functions are reported. In the analysis of the peak positions one can focus, without loss of generality, on the FPMD results of either one of the two FPMD sets, say FPMD(1). The first peak in $g_{tot}^{FPMD(1)}(r)$ is largely due to the Ge−S bonds as shown by the correspondence with the first, very intense peak of $g_{GeS}^{FPMD(1)}(r)$. The second peak of $g_{tot}^{FPMD(1)}(r)$, located at 2.91 Å, stems from the presence of Ge−Ge correlations through edge-sharing (ES) tetrahedra. Indeed, at the distance of 2.91 Å the second peak of $g_{GeGe}^{FPMD(1)}(r)$ is associated with the distance between Ge atoms in fourfold rings (edge-sharing connections). The third peak of our PCF can be attributed mainly to S−S correlations, as indicated by the location of the second peak of $g_{SS}^{FPMD(1)}(r)$ at 3.61 Å.

Considering the partial pair correlation functions, the very intense first peaks characterize $g_{GeS}^{FPMD(1)}(r)$, $g_{GeS}^{FPMD(2)}(r)$, and $g_{GeS}^{HFMD}(r)$, in line with predominant tetrahedral Ge−S heteropolar bonding. The most striking difference between the two sets (FPMD and HFMD) of pair correlation functions rests in the unambiguous presence of Ge−Ge and S−S homopolar bonds in the FPMD case, while the HFMD case features much lower intensities, as visible from the heights of the first peaks in $g_{GeGe}^{HFMD}(r)$ and $g_{SS}^{HFMD}(r)$. This is a first indication of a different bonding nature between the two DFT approaches, HFMD favoring a higher ionic character that prevents from a substantial amount of chemical disorder (deviations from a tetrahedral network). As customarily found in the Ge-Ge pair correlation function of other chalcogenides (GeS_2, GeS_4, SiS_2),[12,20,38] the three peak structure of $g_{GeGe}^{FPMD(1)}(r)$, $g_{GeGe}^{FPMD(2)}(r)$, and $g_{GeGe}^{HFMD}(r)$ is due (going to larger distances) to homopolar Ge−Ge bonds, Ge atoms involved in edge-sharing connections, and Ge atoms involved in corner-sharing (CS) connections. The only sizable difference between the FPMD(1) and the FPMD(2) sets of results is found in the heights of the third peak in $g_{GeGe}^{FPMD(1)}(r)$ and $g_{GeGe}^{FPMD(2)}(r)$ [5% higher in the FPMD(2) case]. Finally, it is of interest to note that each of the three FPMD partial correlation functions has a distinct value for the first minimum: $g_{GeGe}^{FPMD}(r) = 2.68$ Å, $g_{GeS}^{FPMD}(r) = 2.86$ Å, $g_{SS}^{FPMD}(r) = 2.58$ Å. These cutoffs have been employed to produce the forthcoming structural analyses.

B. Coordination numbers and structural units

The coordination numbers $\bar{n}_{\alpha\beta}$ for the HFMD and the FPMD models of g-GeS_2 are listed in Table II. They are defined as the mean number of nearest neighbors of type β around an atom of type α within the integration ranges defined above and corresponding to the first minimum of the appropriate partial correlation functions. For reference purposes, the case of g-$GeSe_2$ is also listed. The coordination numbers pertaining to two popular models of network structures [random covalent network (RCN) and chemically ordered network (CON)] are also shown.

Deviations from perfect chemical order (corresponding to the CON model) are larger for the FPMD cases, in line with the fact that the HFMD approach provides a structure more ionic than the FPMD one. Indeed, while both the FPMD and the HFMD frameworks are broadly consistent

TABLE II. Atomic coordinations for the RCN and CON models for the AX_2 system, compared to the results from our FPMD calculations and previous Harris functional MD calculation[9] for a-GeS_2, and to recent results obtained for the $GeSe_2$ glassy system.[13] For the present works, FPMD(1) and FPMD(2), the cutoffs used are 2.68, 2.86, and 2.58 Å for, respectively, the Ge−Ge, Ge−S, and S−S bonds.

			a-GeS_2			a-$GeSe_2$
	RCN	CON	HFMD	FPMD(1)	FPMD(2)	FPMD[13]
n_{GeGe}	2	0	0.04	0.17	0.13	0.28
n_{GeX}	2	4	3.91	3.62	3.68	3.64
n_{XGe}	1	2	1.96	1.81	1.84	1.82
n_{XX}	1	0	0.05	0.23	0.21	0.20

with a predominant tetrahedral coordination, the number of homopolar bonds is much larger within the fully self-consistent DFT approach. Interestingly, the coordination numbers of g-GeS_2 and g-$GeSe_2$ are quite similar, suggesting that any difference in the bonding character between these two systems cannot be easily highlighted by this kind of structural analysis. To provide a more complete description of short-range order, we identify the individual α-l structural units where an atom of species α (Ge or Se) is l-fold coordinated to other atoms. To clarify this notation, Ge-GeS_2 represents a Ge atom that is connected to one other Ge atom and two S atoms while Ge-S_4 represents a Ge atom that is connected to four S atoms. Results are reported in Table III.

In Ref. 39, it was pointed out that the short-range environments of the Ge and S subnetworks differ profoundly. While the overwhelming majority of the Ge atoms are fourfold coordinated to S atoms, non-negligible proportions of S atoms onefold and threefold coordinated do exist, as made explicit in Table III. Therefore, it appears that the Harris functional framework favors dissimilar charge transfer effects between Ge and S, the first behaving essentially as a positively charged Ge^{4+} ion, while the S atoms can stand different valence states, resulting in distinct nearest neighbor coordinations. In the current FPMD cases, both the Ge and S subnetworks are highly defective, with as many as 30% of the Ge atoms deviating from the fourfold coordination to Se atoms. In this respect, the FPMD descriptions of g-GeS_2 and g-$GeSe_2$ are very much alike, the percentages of Ge atoms twofold and threefold coordinated being very similar. Turning to the S coordinations, the FPMD framework results in a larger number of S atoms twofold coordinated than in the HFMD case, the main difference lying in the vanishing number of S atoms linked to one Ge neighbor, drastically smaller than the 14.3% found within HFMD. Globally, the counting of the structural units is more instrumental to underscore the different topologies of g-GeS_2 emerged from the HFMD and FPMD frameworks, since the percentage of Ge fourfold coordinated to S atoms is drastically higher in the former case. Focusing on the nature of bonding and the amount of chemical order when comparing the structural units of g-GeS_2 and g-$GeSe_2$, the FPMD sets of data are less conclusive, both systems exhibiting a coexistence between the predominant tetrahedron and a conspicuous amount of miscoordinations.

TABLE III. Percentage of l-fold coordinated atoms, decomposed in terms of each specific unit $\bar{n}_\alpha(l)$, in a-GeS_2 (present FPMD works and previous HFMD calculations), and a-$GeSe_2$ from Ref. 13.

		Proportion $\bar{n}_\alpha(l)$ (%)			
		a-GeS_2			a-$GeSe_2$
		HFMD	FPMD(1)	FPMD(2)	FPMD
Ge atom					
$l=2$					
	X_2	1.37	5.8	5.0	3.1
	Ge_1X_1	0.0	0.2	0.0	0.0
$l=3$					
	Ge_1X_2	<0.1	1.6	1.0	1.4
	X_3	1.44	8.3	9.0	5.4
$l=4$					
	Ge_1X_3	3.70	11.6	10.6	12.8
	Ge_2X_2	<0.1	1.4	0.6	2.3
	X_4	93.1	70.5	73.0	72.9
$l=5$					
	Ge_1X_4	<0.1	0.4	0.2	0.0
	X_5	0.0	0.2	0.5	0.0
X = S,Se atom					
$l=1$					
	Ge_1	14.3	0.8	0.6	0.2
$l=2$					
	X_2	0.0	2.5	2.2	2.5
	X_1Ge_1	3.07	17.7	16.0	15.3
	Ge_2	67.9	73.9	76.2	82.8
$l=3$					
	X_2Ge_1	<0.1	0.2	0.0	0.0
	X_1Ge_2	1.81	0.5	0.3	0.0
	Ge_3	12.8	4.5	4.7	1.4

C. Ring statistics

The connectivity profiles for a-GeS_2 shown in Fig. 3 are evaluated by employing the Rigorous Investigation of Networks Generated using Simulation (RINGS) code.[40,41]

Without loss of generality, the following analysis refers to the three trajectories concurring to the FPMD(1) results only. Cutoff distances to determine nearest neighbors are those previously defined (Sec. III A). The analysis is performed by making a King[42]-Franzblau[43] shortest path search to find rings containing a maximum of 30 atoms. In our procedure, we considered all atoms as initial points to begin the search for a given ring, while homopolar bonds are also taken into account. We define $R_c(n)$ as the number of rings containing n atoms (Ge or S) and $P_n(n)$ as the number of atoms that can be used as the origin of search for at least one ring containing n atoms. Both quantities are normalized to the total number of atoms in our model.

The first information given by Fig. 3 is the existence of odd-membered rings in all sizes between three and 30 atoms. This result is due to the presence of S−S and Ge−Ge homopolar bonds. The behavior of $R_c(n)$ is characterized by two distinct patterns [Fig. 3(a)]. For relatively low values of n, two peaks are noticeable, corresponding to small rings containing between four and six atoms. The peak at four is due to ES connections between tetrahedra, whereas the peak at six can be associated with CS connections between

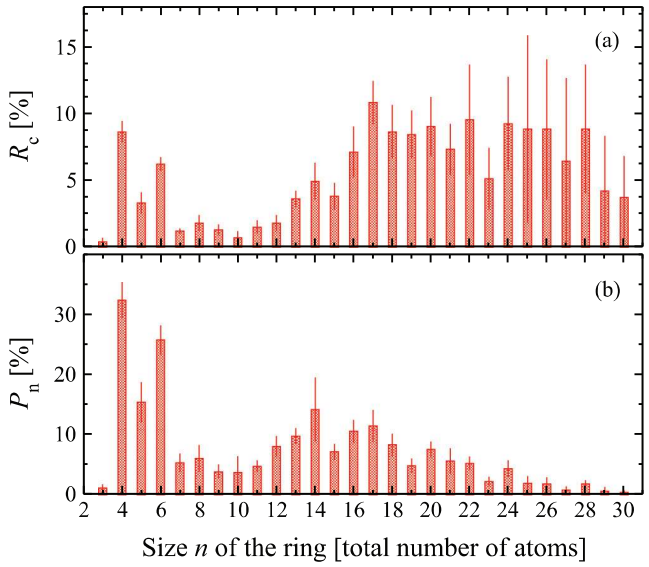

FIG. 3. (Color online) Connectivity profiles, including standard deviations, for a-GeS_2 calculated using the RINGS method.[40,41] (a) $R_c(n)$, number of rings of size n normalized to the total number of atoms in the model; (b) $P_n(n)$, number of atoms at the origin of at least one ring of size n normalized to the total number of atoms in the model.

3 GeS_4 tetrahedra. For n comprised between 10 and 30, a fairly broad distribution becomes visible, with a maximum around 20 atoms per ring.

Focusing on the network picture provided by $P_n(n)$ [Fig. 3(b)], one notices that rings containing four to six atoms are the shortest paths for, respectively, a third and a fourth of all atoms in a-GeS_2 [see Fig. 3(b)]. Therefore, it is legitimate to consider that these rings are the basic building blocks of the topological network in a-GeS_2, although some larger ring sizes (as $n = 14$) do involve more than 10% of the atoms.

The chemical compositions of rings containing $n = n(\mathrm{Ge}) + n(\mathrm{S})$ atoms are listed in Table IV where n(Ge) and n(S) represent the number of Ge and S atoms in a ring, respectively. In the case of even-membered rings, the majority is clearly characterized by $n(\mathrm{Ge}) = n/2$. This remains true for all ring sizes even though the influence of homopolar bonds increases with the size of the ring as the proportion of rings with $n(\mathrm{Ge}) \neq n(\mathrm{S})$ increases. In the case of odd-membered rings, the majority are characterized by $n(\mathrm{Ge}) = (n-1)/2$. This remains true for all ring sizes even though, with increasing the size, there are increasing proportions of odd-membered rings containing $n(\mathrm{Ge}) = (n+1)/2$ and $n(\mathrm{Ge}) = (n+1)/2+1$.

Our statistics also provide the number of Ge atoms that belong to zero, one, and two fourfold rings. These Ge atoms are termed Ge(0), Ge(1), and Ge(2) [see Fig. 4(b)]. We derived that 52.3% of the Ge atoms do not belong to fourfold rings, 31.4% belong to a single fourfold ring, and 12.1% belong to two fourfold rings. By summing up Ge(1) and Ge(2), one obtains the number of Ge atoms in edge-sharing configurations, $N_{\mathrm{Ge}}^{\mathrm{th}}(\mathrm{ES}) = 43.5$ %. This value compares favorably with the experimental estimate of $N_{\mathrm{Ge}}^{\mathrm{exp}}(\mathrm{ES}) = 47 \pm 5$ % derived in Ref. 18 by using *in situ* neutron and x-ray diffraction. Also, it

TABLE IV. The percentage of n-membered rings containing a number n(Ge) of Ge atoms. For example, when n = 9, 35.5% of the rings contain four Ge atoms and 55.5% of the rings contain five Ge atoms. The number of S atoms in an n-membered ring is given by n(S) = n - n(Ge).

	Total number of atoms n in a ring																										
n(Ge)	3	4	5	6	7	8	9	10	11	12	13	14	15	16	17	18	19	20	21	22	23	24	25	26	27	28	29	30
1	80.3																											
2	19.7	**98.4**	53.3	6.2	0.5																							
3		1.6	46.7	**92.4**	41.4	10.3	8.8																					
4				1.4	58.0	**87.7**	35.5	21.9	4.0	0.5																		
5						2.0	55.5	**66.5**	33.8	15.6	5.5	2.8																
6							0.1	8.7	55.5	**74.5**	30.5	21.5	12.1		0.1	0.8	0.1											
7								2.9	5.0	9.4	61.9	**65.7**	29.6	19.1	4.1	0.9	0.4	0.8										
8									1.6		2.1	10.0	51.5	**73.2**	49.4	29.4	15.4	4.3	5.4	1.5	0.4	0.1						
9												0.1	6.8	7.8	45.2	**65.1**	52.9	21.6	15.0	2.1	5.5	0.8	0.3	0.4				
10															1.2	3.6	30.1	**63.8**	45.8	12.4	10.3	3.5	2.2	1.8				
11																0.3	1.1	9.4	32.0	**75.1**	49.7	31.1	21.1	12.5		0.2	0.1	
12																			1.7	8.8	30.3	**63.2**	56.3	26.3	11.5	6.1	1.8	
13																			0.1	0.1	3.8	1.3	19.5	**56.9**	37.4	14.0	20.7	
14																							0.7	2.1	47.2	**65.6**	56.2	
15																									3.8	14.1	18.4	**100**
16																											2.7	

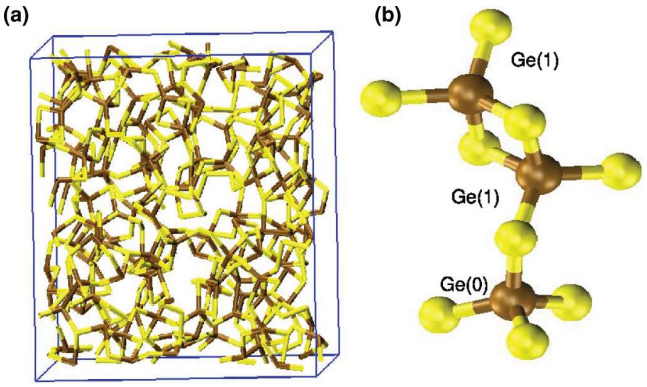

FIG. 4. (Color online) (a) Snapshot of the a-GeS_2 configuration. It is clear the continuous random disposition of tetrahedra which form long chains connecting every region of the material. (b) Example of chain composed by two Ge(1) and one Ge(0) germanium atoms.

underscores a difference with the case of g-$GeSe_2$, for which $N_{Ge}^{th}(ES) = 35\%$.[13]

The identification of Ge atoms belonging to fourfold rings is useful to understand the origins of the major contributions to the first three peaks of the Ge-Ge partial correlation function. The calculation of $g_{GeGe}^{FPMD(1)}(r)$ involving only Ge atoms belonging to (at least) one fourfold ring (i.e., edge-sharing connections) allows highlighting the peak located at ∼3 Å. (see inset of Fig. 2). Conversely, if we account only for Ge atoms that do not belong to any fourfold ring we obtain for $g_{GeGe}^{FPMD(1)}(r)$ and $g_{GeGe}^{FPMD(2)}(r)$ the disappearance of the above feature, the peaks due to homopolar bonds and corner sharing connections being clearly detectable (see inset of Fig. 2).

IV. RECIPROCAL SPACE PROPERTIES

A. Total neutron structure factor and Faber-Ziman partial structure factors

In Fig. 5 we provide a comparison between experimental (Refs. 37 and 18) and calculated total neutron structure

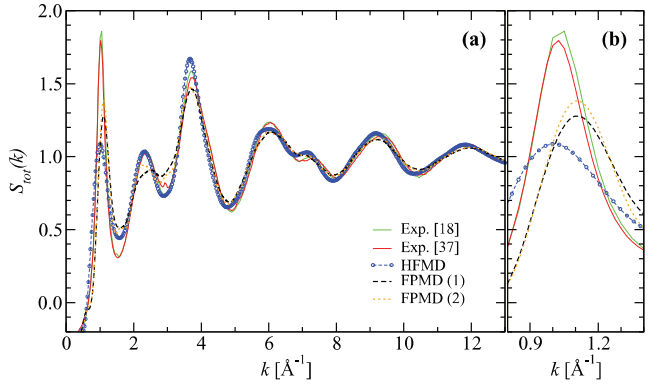

FIG. 5. (Color online) Total structure factor of amorphous GeS_2. Comparison between the HFMD results from Ref. 9 obtained with the Harris functional (blue line), the present FPMD calculations [dashed black and orange lines for, respectively, FPMD(1) and FPMD(2)], and the experimental measurements from Ref. 18 (green line) and Ref. 37 (red line). (a) The overall functions are presented on the left side; (b) a zoom on the FSDP region is presented on the right side.

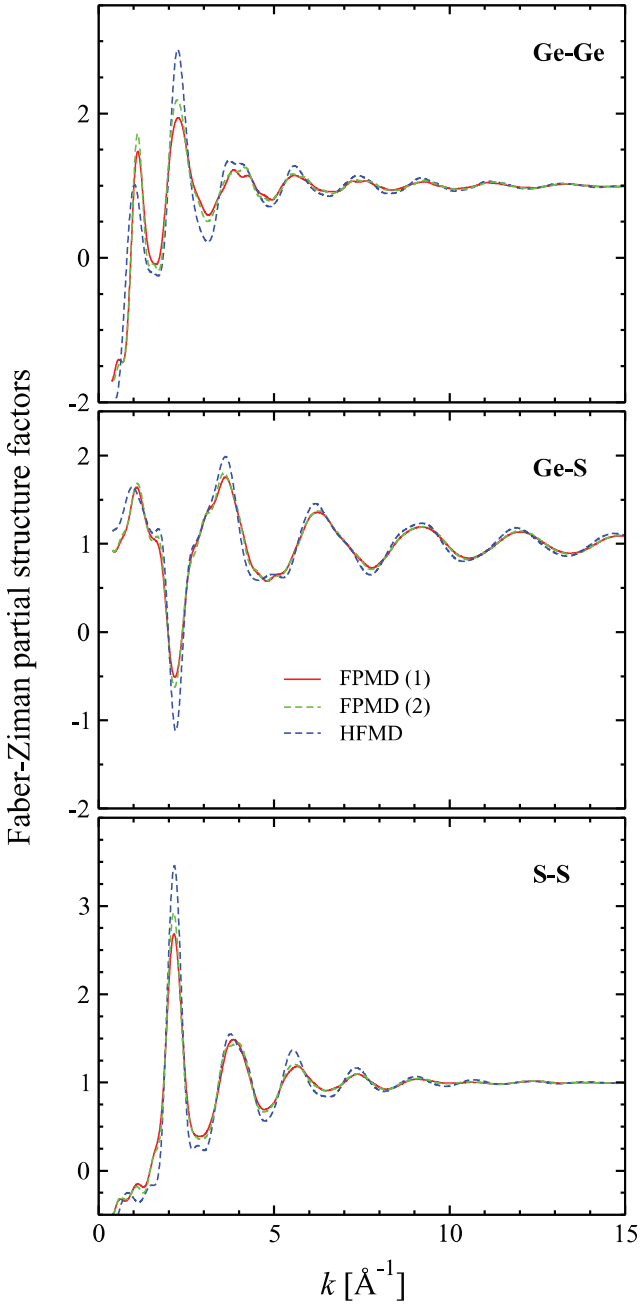

FIG. 6. (Color online) Faber-Ziman structure factors of amorphous GeS_2. Comparison between the results from Ref. 9 obtained with the Harris functional (dashed blue line), and the present FPMD calculations [red line for FPMD(1) and dashed green line for FPMD(2)].

factors $S_T^{\mathrm{FPMD}(1)}(k)$, $S_T^{\mathrm{FPMD}(2)}(k)$, and $S_T^{\mathrm{HFMD}}(k)$. We recall that $S_T^{\mathrm{HFMD}}(k)$ was obtained from the pair correlation functions via a Fourier integration from real space. For the sake of consistency, we employed this same method to obtain $S_T^{\mathrm{FPMD}(1)}(k)$, $S_T^{\mathrm{FPMD}(2)}(k)$ as well as the partial structure factors shown in Figs. 5–7.

While the position of the FSDP is slightly shifted rightward in the FPMD cases, both $S_T^{\mathrm{FPMD}(1)}(k)$ and $S_T^{\mathrm{FPMD}(2)}(k)$ are superior in reproducing the intensities of the peaks over the

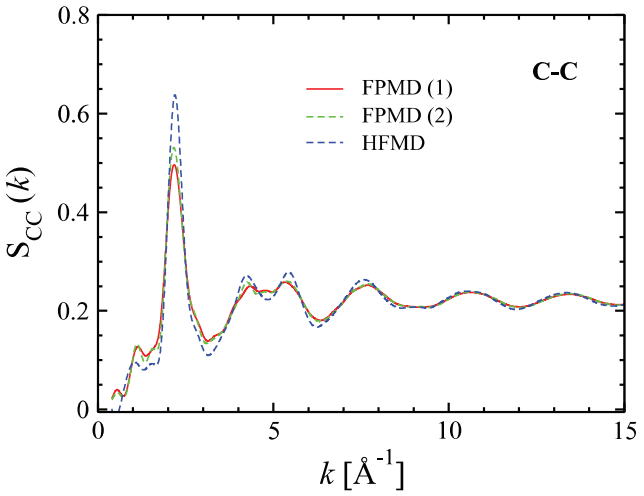

FIG. 7. (Color online) Concentration-Concentration Bhatia-Thornton structure factor of amorphous GeS_2. Comparison between the results from Ref. 9 obtained with the Harris functional (dashed blue line), and the present FPMD calculations [red line for FPMD(1) and dashed green line for FPMD(2)].

entire range of wave vectors. In the low wave vector region, the key to understand this improvement lies in the enhancement of the FSDP for the Faber-Ziman[44] partial structure factor $S_{\mathrm{GeGe}}^{\mathrm{FPMD}}(k)$ [FPMD(1) and FPMD(2)] compared to $S_{\mathrm{GeGe}}^{\mathrm{HFMD}}(k)$ (see Fig. 6). For the Ge-S and S-S partial structure factors, the trends of the FPMD and HFMD in the FSDP region are very similar. One observes that the FSDP is absent in the partial structure factors $S_{\mathrm{SS}}^{\mathrm{FPMD}(1)}(k)$, $S_{\mathrm{SS}}^{\mathrm{FPMD}(2)}(k)$, and $S_{\mathrm{SS}}^{\mathrm{HFMD}}(k)$. Also, similar intensities at the FSDP location are found in $S_{\mathrm{GeS}}^{\mathrm{FPMD}(1)}(k)$, $S_{\mathrm{GeS}}^{\mathrm{FPMD}(2)}(k)$, and $S_{\mathrm{GeS}}^{\mathrm{HFMD}}(k)$.

Our results indicate that the intermediate range order manifests itself more strongly through the appearance of the FSDP when the deviations from chemical order (homopolar bonds, miscoordinations) involve both the Ge and the S subnetworks. This is exactly the case of the FPMD results. On the contrary (HFMD case), the intensity of the FSDP is reduced, in the Ge partial structure factor and the total one, for a network where the overwhelming majority of the Ge atoms is fourfold coordinated to four S atoms.

B. Bhatia-Thornton partial structure factors

In Fig. 7, we focus on the Bhatia-Thornton $S_{\mathrm{CC}}(k)$ (concentration-concentration).[45] The Bhatia-Thornton concentration-concentration partial structure factor $S_{\mathrm{CC}}(k)$ is defined as

$$S_{\mathrm{CC}}(k) = c_{\mathrm{Ge}}c_{\mathrm{Se}}\{1 + c_{\mathrm{Ge}}c_{\mathrm{Se}}[(S_{\mathrm{GeGe}}(k) - S_{\mathrm{GeSe}}(k)) + (S_{\mathrm{SeSe}}(k) - S_{\mathrm{GeSe}}(k))]\}. \quad (4)$$

This quantity expresses the sensitivity to chemical disorder and accounts for contributions due to the chemical environment of each atom.[46] Therefore, it provides information on the fluctuations of concentration associated to the specific value of k. The presence of a non-negligible feature at the FSDP location in both the HFMD and the FPMD sets of data is consistent with the previously identified relationship between

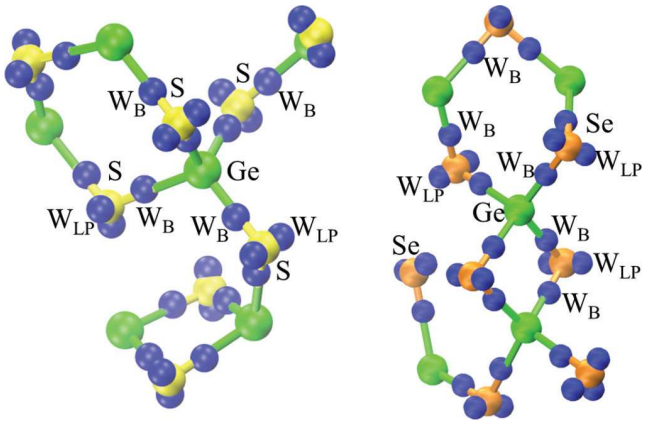

FIG. 8. (Color online) Details of the local bonding environment in the case of GeS_2 (left panel) and $GeSe_2$ (right panel). Ge atoms are shown in green, whereas S and Se atoms are in yellow and orange, respectively. The Wannier centers are the blue balls in both panels. To avoid confusion only a few atoms are labeled, along with representative Wannier centers.

a small departure from chemical order and the appearance of the FSDP.[24] By small departure it has to be intended a deviation from chemical order compatible with the existence of a largely predominant structural motif, as the tetrahedron in the case of A_xX_{1-x} chalcogenides. Indeed, a FSDP in $S_{CC}(k)$ appears in a large variety of disordered model systems exhibiting sizable and yet limited departures from chemical order due to both homopolar bonds and miscoordinations.[13,20,22,38,47]

V. ELECTRONIC PROPERTIES

An analysis of the local electronic structure in terms of maximally localized Wannier functions and centers[35,36] has shed some light on the nature of the chemical bonding in the cases of GeS_2 and $GeSe_2$. Their intrinsic localized distribution in space allows one to infer the extent of covalent vs ionic nature of bonding, via the analysis of the distances between the atomic positions and the centers positions.

As shown in Fig. 8, two types of Wannier functions centers (WFCs) have been identified. The first type, labeled as W_B, refers to the electrons participating to the chemical Ge–S or Ge–Se bonds. The second type, labeled as W_{LP}, indicates instead the lone pair (LP) valence electrons not participating to chemical bonds but remaining localized in the vicinity of the group VI tetra-valent atoms (S, Se). In both cases, the location of the W_B centers with respect to the Ge atoms turns out to be rather similar, being Ge–W_B $= 1.331 \pm 0.010$ Å and Ge–W_B $= 1.351 \pm 0.008$ Å for GeS_2 and $GeSe_2$, respectively. However, assuming as a reference the group VI elements, significant differences arise.

On a first instance, we remark that the distances of W_B centers are shorter for in the case of S, being S–W_B $= 0.859 \pm 0.012$ Å and Se–W_B $= 1.006 \pm 0.005$ Å. This indicates a higher ionic character of the GeS_2 disordered material as opposed to $GeSe_2$.

The above picture is confirmed by the analysis of the LPs in the two glasses. In the case of g-GeS_2, the corresponding WFCs are closer to the group VI element. In fact these distances amount to S–W_{LP} $= 0.427 \pm 0.006$ Å and Se–W_{LP} $= 0.470 \pm 0.009$ Å. As a consequence, the spread associated to the LPs is larger for S (1.880 ± 0.011 Å) than for Se (1.245 ± 0.009 Å).

The general picture provided by this comparative WFCs analysis allows one then to infer that g-GeS_2 is characterized by a more ionic bonding with respect to g-$GeSe_2$. The question arises on the existence of a correlation between this feature and the larger number of edge-sharing units found in g-GeS_2. A qualitative rationale lies on the consideration that edge-sharing connections optimize the packing of pseudocharges of opposite sign through the formation of rings. This is particularly true for systems highly polarizable as g-GeS_2 and g-$GeSe_2$. Therefore, a higher ionic behavior will tend to favor the formation of edge-sharing units.[48]

VI. CONCLUSIONS

The present first-principles molecular dynamics study, focused on the structural properties of g-GeS_2, had two main purposes. First, we intended to provide a set of benchmark results within the framework of a fully self-consistent density functional approach (FPMD), for which a converged plane-wave basis set has been employed. Second, we aimed at a comparison between the topology of g-GeS_2 and g-$GeSe_2$ by exploiting the same theoretical framework. This allows one to ascertain whether there are substantial differences in the bonding character between g-GeS_2 and g-$GeSe_2$. To this purpose, we have generated four independent trajectories for a glass model made of 480 atoms. The first three trajectories are characterized by a very high quench rate ($q(1)_r^{FPMD} = 5 \times 10^{14}$ K/s), while in the fourth one the quench rate has been reduced by more than a factor 10 ($q(2)_r^{FPMD} = 3 \times 10^{13}$ K/s). The close values obtained for the resulting structural properties rule out any strong dependence on the quench rate, at least for the ranges of magnitudes accessible to our computational scheme.

For g-GeS_2, the only available density functional-based result had been produced in the past via the Harris functional scheme (HFMD), combined with a minimal basis set. Despite a strong resemblance between the FPMD and HFMD sets of pair correlation functions, differences are found in the short-range environment of the Ge atoms, strongly tetrahedral within HFMD and highly defective in the FPMD case. Analysis of the total neutron structure factor shows that FPMD improves the intermediate range description of g-GeS_2, as shown by the more intense FSDP feature. When comparing g-GeS_2 and g-$GeSe_2$, it appears that partial (species sensitive) and total coordination numbers cannot be taken as indicative of a different bonding nature. To this purpose, an electronic structure scheme based on the Wannier functions and centers has been applied to representative configurations of g-GeS_2 and g-$GeSe_2$. We found that g-GeS_2 is more ionic than its g-$GeSe_2$ counterpart, in line with previous experimental evidence.

ACKNOWLEDGMENTS

Computational resources have been provided by the Italian National Agency for New Technology, Energy and Sustainable

Economic Development (ENEA) under the ENEA-GRID CRESCO project (www.cresco.enea.it). We warmly acknowledge ENEA for both the technical support and the access to the computational infrastructure. We also acknowledge computational resources allocated from GENCI (Grand Equipement National de Calcul Intensif).

[1] P. Boolchand and W. J. Bresser, Nature (London) **410**, 1070 (2001).
[2] C. C. Huang, D. W. H. Hewak, and J. V. Badding, Opt. Express **12**, 2501 (2004).
[3] K. Naohiko, F. Tatsuo, T. Yasuhiko, T. Akihiro, M. Tomoyoshi, and K. Shoichi, J. Appl. Phys. **100**, 113115 (2006).
[4] J. Málek and J. Shánelová, J. Non-Cryst. Solids. **243**, 116 (1999).
[5] V. Sousa, Microelectron. Eng. **88**, 807 (2011).
[6] I. Valov, R. Waser, J. R. Jameson, and M. N. Kozicki, Nanotechnology **22**, 254003 (2011).
[7] C. Gopalan, Y. Ma, T. Gallo, J. Wang, E. Runnion, J. Saenz, F. Koushan, P. Blanchard, and S. Hollmer, Solid-State Electron. **58**, 54 (2011).
[8] S. Blaineau, P. Jund, and D. A. Drabold, Phys. Rev. B **67**, 094204 (2003).
[9] S. Le Roux and P. Jund, J. Phys.: Cond. Mat. **19**, 196102 (2007).
[10] M. Cobb, D. A. Drabold, and R. L. Cappelletti, Phys. Rev. B **54**, 12162 (1996).
[11] L. Giacomazzi, C. Massobrio, and A. Pasquarello, Phys. Rev. B **75**, 174207 (2007).
[12] M. Micoulaut, R. Vuilleumier, and C. Massobrio, Phys. Rev. B **79**, 214205 (2009).
[13] A. Bouzid and C. Massobrio, J. Chem. Phys. **137**, 046101 (2012).
[14] S. R. Elliott, Phys. Rev. Lett. **67**, 711 (1991).
[15] I. Petri, P. S. Salmon, and H. E. Fischer, Phys. Rev. Lett. **84**, 2413 (2000).
[16] I. Petri and P. S. Salmon, J. Non-Cryst. Solids. **293–295**, 169 (2001).
[17] L. Cai and P. Boolchand, Phil. Mag. B **82**, 1649 (2002).
[18] A. Ziedler, W. E. Drewitt, P. S. Salmon, A. C. Barnes, W. A. Crichton, S. Klotz, H. E. Fischer, C. J. Benmore, S. Ramos, and A. C. Hannon, J. Phys.: Cond. Mat. **21**, 474217 (2009).
[19] O. F. Sankey and D. J. Niklewski, Phys. Rev. B **40**, 3979 (1989).
[20] C. Massobrio, M. Celino, P. S. Salmon, R. A. Martin, M. Micoulaut, and A. Pasquarello, Phys. Rev. B **79**, 174201 (2009).
[21] K. Sykina, E. Furet, B. Bureau, S. Le Roux, and C. Massobrio, Chem. Phys. Lett. **547**, 30 (2012).
[22] S. Le Roux, A. Bouzid, M. Boero, and C. Massobrio, Phys. Rev. B **86**, 224201 (2012).
[23] M. Micoulaut, S. Le Roux, and C. Massobrio, J. Chem. Phys. **136**, 224504 (2012).
[24] C. Massobrio and A. Pasquarello, Phys. Rev. B **77**, 144207 (2008).
[25] R. Car and M. Parrinello, Phys. Rev. Lett. **55**, 2471 (1985).
[26] Computer code CPMD, Version 3.15 [http://www.cpmd.org], IBM Corp., Armonk, NY, 1990–2013 and MPI für Festkörperforschung Stuttgart, Stuttgart, 1997–2001.
[27] P. Boolchand, J. Grothaus, M. Tenhover, M. A. Hazle, and R. K. Grasselli, Phys. Rev. B **33**, 5421 (1986).
[28] A. D. Becke, Phys. Rev. A **38**, 3098 (1988).
[29] C. Lee, W. Yang, and R. G. Parr, Phys. Rev. B **37**, 785 (1988).
[30] J. P. Perdew and Y. Wang, Phys. Rev. B **45**, 13244 (1992).
[31] N. Troullier and J. L. Martins, Phys. Rev. B **43**, 1993 (1991).
[32] S. Nosé, Mol. Phys. **52**, 255 (1984).
[33] W. G. Hoover, Phys. Rev. A **31**, 1695 (1985).
[34] P. E. Blöchl and M. Parrinello, Phys. Rev. B **45**, 9413 (1992).
[35] N. Marzari and D. Vanderbilt, Phys. Rev. B **56**, 12847 (1997).
[36] R. Resta and S. Sorella, Phys. Rev. Lett. **82**, 370 (1999).
[37] E. Bychkov, M. Fourmentin, M. Miloshova, and C. Benmore, in *Proceedings of the ILL Millennium Symposium–Grenoble, France April 6–7* (ILL Neutrons for Science, Grenoble, 2001), p. 54.
[38] M. Celino and C. Massobrio, Phys. Rev. Lett. **90**, 125502 (2003).
[39] S. Blaineau and P. Jund, Phys. Rev. B **69**, 064201 (2004).
[40] S. Le Roux and P. Jund, Comp. Mat. Sci. **49**, 70 (2010).
[41] S. Le Roux and P. Jund, Comp. Mat. Sci. **50**, 1217 (2011).
[42] S. V. King, Nature (London) **213**, 1112 (1967).
[43] D. S. Franzblau, Phys. Rev. B **44**, 4925 (1991).
[44] Y. Waseda, *The Structure of Non-Crystalline Materials* (McGraw-Hill, New-York, 1980); describes the relationship between the three sets of partial structure factors commonly used (Faber-Ziman, Ashcroft-Langreth, and Bhatia-Thornton).
[45] A. B. Bhatia and D. E. Thornton, Phys. Rev. B **2**, 3004 (1970).
[46] P. S. Salmon, Proc. Roy. Soc. London A **437**, 591 (1992).
[47] S. Le Roux, A. Zeidler, P. S. Salmon, M. Boero, M. Micoulaut, and C. Massobrio, Phys. Rev. B **84**, 134203 (2011).
[48] M. Wilson and P. S. Salmon, Phys. Rev. Lett. **103**, 157801 (2009).